An Efficient Method for the Determination of Interfacial Tensions from Drop Profiles

J. W. Jennings, Jr.*

Standard Alaska Production Company, P.O. Box 196193, Anchorage, Alaska 99519-6193

N. R. Pallas

Standard Oil Production Company, 4440 Warrensville Center Road, Cleveland, Ohio 44128

Received July 20, 1987. In Final Form: March 9, 1988

A new method has been developed for the determination of interfacial tensions between two fluids from primary drop shape data. The technique is applicable to either pendant or sessile drops. The required data are limited to the x,z coordinates of the drop profile, the density difference between the two fluids, and the magnification. We build upon the work of Rotenberg et al. (Rotenberg, Y.; Boruvka, L.; Neumann, A. W. *J. Colloid Interface Sci.* **1983**, *93*, 169), whose main innovations were to obviate the accurate measurement of the coordinates of the apex, define the objective function with a line normal from a data point to a calculated drop profile, and use the incrementally loaded Newton–Raphson method. The major difference in the method presented here is the use of rotational discrimination instead of the incrementally loaded Newton–Raphson technique to minimize the objective function. It is shown, by use of numerically generated drop profiles and one set of experimental data for pure water at 25 °C, that this new method is superior to that of Rotenberg et al. on three points. First, it is found that this method requires 4–50 times less processing time per drop profile. Second, a superior error analysis is performed. Third, the new method determines two additional experimental parameters, the aspect ratio and rotational angle of the optical system. Furthermore, by use of the new error analysis, the dependence of the error on the shape of a drop, pendant and sessile, is examined. An "optimum" range of drop shapes is found.

Introduction

The drop shape technique is frequently the method of choice for the determination of interfacial tension at fluid–fluid interfaces. This technique does not rely upon any correction factors, it is mechanically static, it does not rupture the interface, it is able to measure tensions of nearly any magnitude, and the measurements can be made rapidly as a function of time to account for aging. The measurements are contact angle independent and can be performed under extreme conditions of temperature and pressure with little difficulty.

Until recently, the accuracy of the technique depended solely upon the measurement of lengths at certain inflection points on the drop profile.[1-5] With the extensive use of computers now found in many laboratories, it is possible, by numerical integration of the Young–Laplace equation, to use data encompassing an entire drop profile for the determination of interfacial tension. The advantages of numerical analysis of data encompassing an entire drop profile have been discussed elsewhere.[6] Such a technique is especially useful for the accurate determination of ultralow interfacial tensions, where the use of traditional analysis techniques is not applicable or may produce unacceptably large errors.[8] Several such numerical techniques have been reported.[6-10]

However, we find that the best of the numerical techniques available[6] is inadequate on two major points. First, the analysis makes inefficient use of central processor unit (cpu) time. In order to fully investigate some complex interfacial systems, in which the tension changes by 2 orders of magnitude in 2 min, it is necessary to record hundreds of drop profiles. An apparatus based upon a solid-state television camera interfaced to an imaging computer is capable of recording 1 profile/s.[11] In order to compensate for the reduced resolution of a typical solid-state camera it is necessary to record on the order of 1000 coordinates per drop profile. We find that use of the analysis technique of ref 6 may consume 64 h of cpu time in order to analyze a data set consisting of 500 profiles each of 1000 coordinates when run on a VAX 8600 computer. Thus, the need for an analysis technique able to handle vast quantities of data efficiently is clear. An additional advantage of such a technique lies in the ability to reduce the error in the measurement of time-independent tensions by statistical analysis of many profiles. Secondly, the aforementioned technique used a Monte Carlo style error analysis, which occasionally results in confidence intervals that do not bracket the calculated mean.

The optimization technique used in the method herein presented, rotational discrimination,[12] is found to be superior to the previously used Newton–Raphson technique[6] in several respects. The amount of computer time required to analyze the data is reduced 4–50 times with no loss of precision or accuracy. The reduction in processing time permits the experimentalist to observe changes in the interfacial tension with time which otherwise would have been impractical due to the number of the resulting drop profile data sets. The decrease in processing time results in part from the fact that rotational discrimination does not require the second derivatives of the objective function and requires fewer evaluations of the objective function

* Author to whom correspondence should be addressed.

(1) Fordham, S. *Proc. R. Soc. London, A* **1948**, *194*, 1.
(2) Neiderhauser, D. O.; Bartell, F. E. *Am. Pet. Inst. Res. Proj. 27* **1948–1949**, 114.
(3) Winkel, D. *J. Phys. Chem.* **1965**, *69*, 348.
(4) Roe, R. J.; Bachetta, V. L.; Wong, P. M. G *J. Phys. Chem.* **1976**, *71*, 4190.
(5) Lyons, C. J.; Eihing, E.; Wilson, I. R. *J. Chem. Soc., Faraday Trans. 2* **1985**, *81*, 327.
(6) Rotenberg, Y.; Barouka, L.; Neumann, A. W. *J. Colloid Interface Sci.* **1983**, *93*, 169.
(7) Maze, C.; Burnet, G. *Surf. Sci.* **1971**, *24*, 335.
(8) Huh, C.; Reed, R. L. *J. Colloid Interface Sci.* **1983**, *91*, 472.
(9) Butler, J. N.; Bloom, B. H. *Surf. Sci.* **1966**, *4*, 1.
(10) Patterson, R. E.; Ross, S. *Surf. Sci.* **1979**, *81*, 451.
(11) The description and results demonstrating the capabilities of the imaging computer based drop shape apparatus are to be published. However, see: Girault, H. H.; Schiffrin, D. J.; Smith, B. D. V. *J. Electroanal. Chem.* **1982**, *137*, 207.
(12) Law, V. J.; Fariss, R. H. *Ind. Eng. Chem. Fundam.* **1972**, *11*, 154.

0743-7463/88/2404-0959$01.50/0

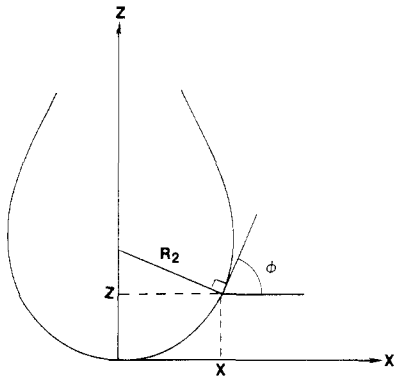

Figure 1. Representation of the drop profile coordinate system.

than does the Newton–Raphson technique.

In this method the confidence limits on the calculated interfacial tension are obtained directly as a part of the optimization instead of through a Monte Carlo technique.[13] The direct calculation of the confidence limits further reduces the processing time. Finally, the method allows two additional experimental parameters to be estimated: the rotational angle of the camera used to view the drop and the aspect ratio (x/z magnification) of the optical system.

Regardless of the optimization technique used, the calculation of the interfacial tension requires as base data the (x,z) coordinates of the drop profile, the magnification factor, the difference in density between the two phases, and the local acceleration due to gravity. The drop profile coordinates may be obtained by manual digitization of the drop image from a photograph or direct observation of the drop image by a closed circuit television camera interfaced to an imaging computer. From this data, the coordinates of the drop profile apex, (X_0, Z_0), and radius of curvature at the apex, R_0, are approximated. Then, given a first guess for the interfacial tension, the routine performs a nonlinear optimization between the observed profile coordinates and profile coordinates obtained by integration of the Young–Laplace equation. The result of the optimization determines the coordinates of the apex, the radius of curvature at the apex, and the interfacial tension and if desired the rotational angle of the optical system and the aspect ratio.

Description of a Drop Profile

The usual form of the equation of Young and Laplace relates the pressure drop across an interface at a given point to the two radii of curvature at that point and the interfacial tension.[14] Following a previous development,[6] the equation of Young and Laplace may be expressed as a set of three first-order differential equations:

$$dx/ds = \cos \phi \quad (1)$$

$$dz/ds = \sin \phi \quad (2)$$

$$d\phi/ds = 2 + \beta z - \sin \phi/x \quad (3)$$

where x and z are the X and Z coordinates of a point on a drop profile reduced to dimensionless variables by division by R_0, the radius of curvature at the apex. Similarly, s is the dimensionless arc length from the apex to the point (x,z), ϕ is the turning angle at that point (Figure 1), and β is defined as

$$\beta = \Delta\rho g R_0^2/\gamma \quad (4)$$

where $\Delta\rho$ is the difference in density between the two phases, g is the local acceleration due to gravity, and γ is the interfacial tension. Simultaneous integration of eq 1–3, subject to the initial condition $x(0) = z(0) = \phi(0) = 0$, yields the functions $x(s)$ and $z(s)$ defining the curve that describes the drop profile.

The functions x, z, and ϕ depend upon the parameter β. The solution to the optimization problem to obtain the interfacial tension requires the functions x' and z', where the prime denotes the partial derivative with respect to β. Differentiating eq 1–3 with respect to β gives

$$dx'/ds = -\phi' \sin \phi \quad (5)$$

$$dz'/ds = \phi' \cos \phi \quad (6)$$

$$\frac{d\phi'}{ds} = z + \beta z' - \frac{\phi' \cos \phi}{x} + \frac{x' \sin \phi}{x^2} \quad (7)$$

with the initial condition $x'(0) = z'(0) = \phi'(0) = 0$.

For a fixed β eq 1–3 and 5–7 form a system of six first-order ordinary differential equations (with the independent variable s) that, together with the initial conditions, can be solved numerically by using the second-order implicit Euler method.[6] Use of this method yields a set of values, x_j, z_j, x'_j, and z'_j, which approximate the functions $x(s)$, $z(s)$, $x'(s)$, and $z'(s)$ at the points s_j. For this application the equally spaced points $s_j = j\Delta s$, $j = 1, 2, 3 \ldots J$, where J is the number of calculated profile coordinates, have been chosen.

The use of the incrementally loaded Newton–Raphson method to find the parameters that give a best fit to the observed drop profile requires the additional functions $x''(s)$ and $z''(s)$. However, the rotational discrimination algorithm used here requires only the functions $x(s)$, $x'(s)$, $z(s)$, and $z'(s)$. This accounts for part of the improved efficiency of the new program.

The Objective Function

The experimental measurement of the profile of a drop results in a set of m data points, (X_i^{obsd}, Z_i^{obsd}), $i = 1, 2, 3, \ldots m$, where X_i^{obsd} and Z_i^{obsd} are the observed coordinates of a point on the drop profile. Of course the observed, magnified coordinates must be scaled to real physical dimensions by use of the experimentally determined magnification factor. If the observed coordinates are obtained by use of an image-processing computer with a closed circuit television camera, the vertical (z) and horizontal (x) magnifications may not be the same. The ratio of the two magnifications defines the aspect ratio, $a = M_x/M_z$. The aspect ratio is a fixed constant of the apparatus, but should be checked experimentally. At least one of the two magnification factors must be known in order to obtain a unique solution by use of the algorithm. However, the aspect ratio can be determined by the algorithm, if desired, providing a check of the consistency of the measurements or for trouble shooting.

The coordinate system in which the data are observed will, in general, be translated with respect to the coordinate system in which the drop profile is calculated since the exact location of the apex is not known. It may also be rotated if the camera is not exactly aligned vertically.

(13) The details of the error analysis were not published in ref 6. However, the computer program made available to us from the authors contained a routine to estimate the confidence limits based upon the generation of small normally distributed changes in the experimental data of a set standard deviation. The "adjusted" experimental data were then reprocessed to obtain the tension. The procedure was repeated seven times in order to obtain an estimate of the interval of the mean with 95% confidence. We found, however, that the mean value was frequently not bracketed by this range, indicating that seven trials are statistically inadequate.

(14) Adamson, A. W. *Physical Chemistry of Surfaces*, 4th ed.; Wiley: New York, 1976.

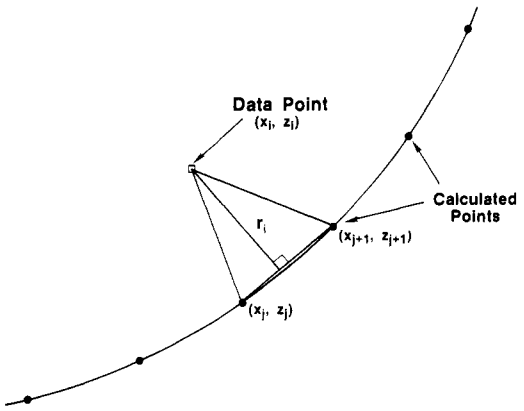

Figure 2. Illustration of the computation of the residuals.

Hence, the data must be rotated and translated as well as scaled.

More explicitly

$$X_i = (X_i^{obsd}/M_x - X_0) \cos\theta + (aZ_i^{obsd}/M_x - Z_0) \sin\theta \quad (8a)$$

$$Z_i = (aZ_i^{obsd}/M_x - Z_0) \cos\theta - (X_i^{obsd}/M_x - X_0) \sin\theta \quad (8b)$$

where (X_0,Z_0) is the coordinate of the apex in real, physical dimensions and θ is the angle of rotation.

The objective function may now be defined by

$$Q = \sum_{i=1}^{m} r_i^2 \quad (9)$$

where

$$r_i = \pm[(X(s_i) - X_i)^2 + (Z(s_i) - Z_i)^2]^{1/2} \quad (10)$$

Equations 9 and 10 define the objective function, Q, as the sum of the squared residuals r_i, where r_i equals the distance between the transformed data point (X_i,Z_i) and the corresponding closest point on the calculated drop shape $(X(s_i),Z(s_i))$. The sign of r_i indicates whether the data point lies inside (+) or outside (−) the calculated profile and has not other bearing on the solution. The values of $(X(s_i),Z(s_i))$ are related to the dimensionless coordinates $(x(s_i),z(s_i))$ by a factor of R_0, as previously mentioned.

Since the coordinates of the calculated drop profile, (x_j,z_j), are obtained at discrete dimensionless arc length intervals Δs, it is unlikely that there will be a point $(x_j,z_j) = (x(s_i),z(s_i))$. Therefore, the point $(x(s_i),z(s_i))$ must be computed by interpolation between the existing points (x_j,z_j). This is done for each transformed data point (X_i,Z_i) by first locating the two nearest computed points, (X_j,Z_j) and (X_{j+1},Z_{j+1}). This step must be performed carefully or large amounts of processing time may be consumed. An effective method is to use a linear search starting from the point on the computed profile closest to the data point i on the previous iteration.

The three points (X_i,Z_i), (X_j,Z_j), and (X_{j+1},Z_{j+1}) form a triangle as shown in Figure 2. The distance r_i may then be computed:

$$r_i \simeq \frac{(Z_j - Z_i)(X_j - X_{j+1}) - (X_j - X_i)(Z_j - Z_{j+1})}{[(X_j - X_{j+1})^2 + (Z_j - Z_{j+1})^2]^{1/2}} \quad (11)$$

Occasionally a line normal to the calculated drop connecting to a given data point may not exist. This may occur for pendant drop data points near the syringe tip early in the computation when the parameter values are not yet close to the final solution. When this occurs the corresponding data points are ignored in the program by setting their residuals and derivatives to zero. When the final solution is approached these points are reincluded in the computation automatically.

Minimization of the Objective Function by Rotational Discrimination

The problem of finding the set of parameters that gives a best fit between the calculated and observed drop shape takes the form of a nonlinear least-squares minimization problem. That is, the value of the vector $\mathbf{U}$ is to be determined such that the objective function $Q(\mathbf{U})$ is minimized, where

$$\mathbf{U} = \begin{bmatrix} U_1 = \theta/w_\theta \\ U_2 = a/w_a \\ U_3 = X_o/w_X \\ U_4 = Z_o/w_Z \\ U_5 = R_o/w_R \\ U_6 = \alpha/w_\alpha \end{bmatrix} \qquad \alpha = 1/\gamma \quad (12)$$

$$Q(\mathbf{U}) = \sum_{i=1}^{m} r_i^2(\mathbf{U}) \quad (13)$$

The values of w in eq 12 are constant scale factors which will be chosen later in order to optimize the performance of the minimization algorithm. The vector $\mathbf{U}$ may also be any nonempty subset of the six parameters. Therefore, the following discussion will refer to the vector $\mathbf{U}$ of length n.

The version of rotational discrimination used here to minimize the objective function is essentially a modified form of the Gauss–Newton technique. Both are iterative methods for obtaining the minimum of a sum-of-squares objective function and assume that the residuals can be approximated at each iteration by planes in the n-dimensional parameter space. Both methods recognize that the minumum of Q occurs at a point $\mathbf{U}^*$ such that $\mathbf{Q}'(\mathbf{U}^*) = 0$, where $\mathbf{U}^*$ is the solution to the minimization problem. $\mathbf{Q}'$ may approximated as a truncated Taylor series about a base point $\mathbf{U}^0$:

$$\mathbf{Q}'(\mathbf{U}) \simeq \mathbf{Q}'(\mathbf{U}^0) + \boldsymbol{Q}''(\mathbf{U}^0)\Delta\mathbf{U} \quad (14)$$

where $\Delta\mathbf{U} = \mathbf{U} - \mathbf{U}^0$. An estimate of the solution of $\mathbf{U}^*$ may be found by setting $\mathbf{U} = \mathbf{U}^*$ in eq 14

$$\mathbf{U}^* \simeq \mathbf{U}^0 - [\boldsymbol{Q}''(\mathbf{U}^0)]^{-1}\mathbf{Q}'(\mathbf{U}^0) \quad (15)$$

This suggests the iterative procedure

$$\mathbf{U}^{k+1} = \mathbf{U}^k + \Delta\mathbf{U}^k; \quad k = 0, 1, 2 \ldots$$

where $\Delta\mathbf{U}^k$ is the solution of

$$\boldsymbol{Q}''(\mathbf{U}^k)\,\Delta\mathbf{U}^k = -\mathbf{Q}'(\mathbf{U}^k) \quad (16)$$

The elements of $\mathbf{Q}'$ may be found by differentiation of the objective function with respect to each of the n elements of $\mathbf{U}$:

$$Q_p'(\mathbf{U}) = \frac{\partial Q(\mathbf{U})}{\partial U_p} = 2\sum_{i=1}^{m} r_i \frac{\partial r_i}{\partial U_p}; \quad p = 1 \ldots n \quad (17)$$

Similarly

$$Q_{pq}''(\mathbf{U}) = \frac{\partial^2 Q(\mathbf{U})}{\partial U_p \partial U_q} = 2\sum_{i=1}^{m} \frac{\partial r_i}{\partial U_p}\frac{\partial r_i}{\partial U_q} + 2\sum_{i=1}^{m} r_i \frac{\partial^2 r_i}{\partial U_p \partial U_q}$$

which may be approximated by

$$Q_{pq}''(\mathbf{U}) \simeq 2\sum_{i=1}^{m} \frac{\partial r_i}{\partial U_p}\frac{\partial r_i}{\partial U_q}; \quad p,q = 1 \ldots n \quad (18)$$

The partial derivatives of the residuals with respect to the elements of $\mathbf{U}$ are given in the Appendix. The computa-

tional advantages of using the approximation defined by eq 18, as pointed out by Nolen,[15] are as follows: (1) Only first-order derivatives of r_i need be computed. (2) Equation 18 gives a good approximation of $\boldsymbol{Q}''$ near a minimum of Q but gives a poor approximation near a maximum or saddle point. This causes the procedure to pass quickly through maxima and saddle points, converging only to a minimum.

The geometric interpretation of these equations is that the residuals r_i have been approximated by planes in an n-dimensional space. Q has been approximated near $\mathbf{U}^k$ by an n-dimensional paraboloid that is everywhere convex upward. The vector $\Delta\mathbf{U}^k$ of eq 16 moves from the base point $\mathbf{U}^k$ to the minimum of that paraboloid.

Rotational discrimination departs from the Gauss–Newton method as follows.[15] Decomposing $\boldsymbol{Q}''(\mathbf{U}^k)$ gives

$$\boldsymbol{T}^T(\mathbf{U}^k)\ \boldsymbol{Q}''(\mathbf{U}^k)\ \boldsymbol{T}(\mathbf{U}^k) = \boldsymbol{E}(\mathbf{U}^k) \tag{19}$$

where $\boldsymbol{E}(\mathbf{U}^k)$ is an $n \times n$ diagonal matrix whose elements are the eigenvalues of $\boldsymbol{Q}''(\mathbf{U}^k)$ and $\boldsymbol{T}(\mathbf{U}^k)$ is an orthogonal $n \times n$ matrix whose columns are the corresponding eigenvectors of $\boldsymbol{Q}''(\mathbf{U}^k)$. Since $\boldsymbol{Q}''(\mathbf{U}^k)$ is a symmetric matrix, its eigenvalues and eigenvectors can be computed by using Jacobi's method (see, for example, Carnahan, Luther, and Wilkes[16]). Also, since $\boldsymbol{T}(\mathbf{U}^k)$ is orthogonal

$$\boldsymbol{T}(\mathbf{U}^k)\ \boldsymbol{T}^T(\mathbf{U}^k) = I \tag{20}$$

Equation 16 can now be written as

$$\boldsymbol{T}^T(\mathbf{U}^k)\ \boldsymbol{Q}''(\mathbf{U}^k)\ \boldsymbol{T}(\mathbf{U}^k)\ \boldsymbol{T}^T(\mathbf{U}^k)\ \Delta\mathbf{U}^k = -\boldsymbol{T}^T(\boldsymbol{U}^k)\ \mathbf{Q}'(\mathbf{U}^k) \tag{21}$$

Rotational discrimination uses a change of coordinate system from $(U_1, U_2, \ldots U_n)$ to $(V_1, V_2, \ldots V_n)$, where $\boldsymbol{T}^T(\mathbf{U}^k)$ is the transformation matrix

$$\mathbf{V}(\mathbf{U}) = \boldsymbol{T}^T(\mathbf{U}^k)\ (\mathbf{U} - \mathbf{U}^k) \tag{22}$$

The vector $\mathbf{V} = (V_1, V_2 \ldots V_n)$ defines a new rotated orthogonal coordinate system whose origin is at $\mathbf{U}^k$. It can be shown that the gradient vector of Q with respect to $\mathbf{V}$ is

$$(\partial\mathbf{Q}/\partial\mathbf{V})(\mathbf{U}) = \boldsymbol{T}^T(\mathbf{U}^k)\ \mathbf{Q}'(\mathbf{U}) \tag{23}$$

Substituting eq 19, 22, and 23 into eq 21 gives

$$\boldsymbol{E}(\mathbf{U}^k)\ \mathbf{V}(\mathbf{U}^k) = -(\partial\mathbf{Q}/\partial\mathbf{V})(\mathbf{U}^k) \tag{24}$$

Since the only non-zero elements of $\boldsymbol{E}$ are on the diagonal, eq 24 can be rearranged, giving

$$V_p = -(\partial Q/\partial V_p)/E_{pp} \tag{25}$$

where E_{pp} are the elements on the diagonal of $\boldsymbol{E}(\mathbf{U}^k)$ (the eigenvalues of $\boldsymbol{Q}''(\mathbf{U}^k)$). The desired vector $\Delta\mathbf{U}^k$ can now be computed from eq 22:

$$\Delta\mathbf{U}^k = \boldsymbol{T}(\mathbf{U}^k)\ \mathbf{V}(\mathbf{U}^k) \tag{26}$$

At this point it is helpful to make some observations concerning the geometric interpretation of eq 19–26. The eigenvectors of $\boldsymbol{Q}''(\mathbf{U}^k)$ are the principal axes of the paraboloid that approximates Q near $\mathbf{U}^k$. The eigenvalues $\boldsymbol{Q}''(\mathbf{U}^k)$ are the second derivatives of the paraboloid in the eigenvector directions. Since the paraboloid is everywhere concave upward, the eigenvalues are always positive. The vectors $\Delta\mathbf{U}^k$ and $\mathbf{V}(\mathbf{U}^k)$ are representations of the same vector in two different coordinate systems. The vector $\Delta\mathbf{U}^k$ points from $\mathbf{U}^k$ toward the minimum of the paraboloid in the parameter coordinate system. The vector $\mathbf{V}(\mathbf{U}^k)$ points from $\mathbf{U}^k$ toward the minimum of the paraboloid in an orthogonal coordinate system whose origin is at $\mathbf{U}^k$ and whose axes are parallel to the eigenvectors. In other words, $\mathbf{V}(\mathbf{U}^k)$ is expressed in a coordinate system that has been rotated to coincide with the principle axes of the paraboloid. Law and Fariss refer to this rotated coordinate system as "non-interacting". That is, the change in Q caused by moving a distance V_i in one of the eigenvector directions is independent of the distances moved in the other eigenvector directions.

If eq 25 is used without modification, then eq 26 recovers the Gauss–Newton method exactly. However, in the implementation of rotational discrimination eq 25 is modified to avoid the problems of large oscillations and large moves in null-effect directions present in the Gauss–Newton method.[11]

The problem of large oscillations is in part remedied by limiting the maximum move permitted in any eigenvector direction. This is permissible because the eigenvector coordinate system is noninteracting. In contrast, such limiting in the Gauss–Newton method may lead to slow convergence or divergence.

The Guass–Newton method will usually produce very large moves in null-effect directions. Null-effect vectors may easily be detected by comparison of the eigenvalues. Any eigenvalue many orders of magnitude smaller than the largest eigenvalue indicates that Q is nearly flat for appropriately scaled problems. Any move in the corresponding eigenvector direction will be null-effect. A better strategy, adopted in rotational discrimination, is to not move at all in these directions.

Implementation

A number of details remain to be discussed concerning the implementation of rotational discrimination. In order for rotational discrimination to work well the scale factors and the maximum jump parameter, V_{max}, need to be chosen appropriately. Since each element of the vector $\mathbf{V}$ is compared to the same value V_{max}, the region in which the parameter search is conducted should be roughly an n-dimensional cube. If the search region is several orders of magnitude smaller in one parameter direction than the others, a V_{max} small enough to prevent oscillations in the direction of that parameter will overly restrict the permissible jump size in the other directions. In the extreme case a parameter can be erroneously identified as locally null-effect. An ideal situation would be one in which the solution is at the center of a unit cube in n dimensions and the initial guess is at one of the corners. In practice, the ideal situation need only be approximated to within about 1 order of magnitude for the algorithm to perform well. As a rule of thumb the scale factors should be roughly equal to the distance each initial guess is likely to be from its corresponding value at the solution. The following choices have been used with good results on a wide variety of problems encompassing nearly all possible drop shapes, both pendant and sessile: $w_\theta \simeq 2°$, $w_a \simeq 0.1$, $w_X = w_Z \simeq 10\%$ of the drop width, $w_R \simeq 40\%$ of the drop width, $w_\alpha \simeq 80\%$ of the initial guess, and $V_{max} \simeq 0.2$.

Limiting the maximum permitted move is accomplished in the program by comparing the absolute value of each V_p computed by eq 25 to the maximum value V_{max}. If the magnitude of V_p is larger than V_{max}, then the magnitude of V_p is reset to V_{max} and its algebraic sign retained. Law and Fariss recommend a more sophisticated procedure for handling the V_p values involving the method of "weighted

(15) Nolen, J. S., private communication, 1983.
(16) Carnahan, B.; Luther, H. A.; Wilkes, J. O. *Applied Numerical Methods*; Wiley: New York, 1969; pp 250–260.

steepest descent". In this work, however, the method described above has performed well and has been retained in the interest of simplicity.

The program detects null-effect vectors by examining the ratios E_{pp}/E_{max}, where E_{max} is the largest eigenvalue of $\boldsymbol{Q}''(\mathbf{U}^k)$. Whenever this ratio is smaller than $E_{null} = 1 \times 10^{-6}$, the corresponding V_p is set to zero.

Since each iteration of the objective function minimization process involves the approximation that each r_i is a plane in n-dimensional space, any parameter transformation that improves this approximation will result in faster convergence. Numerical experimentation with the drop fitting problem has shown that the residuals are approximately linear functions of the first five parameters, and no transformation is needed. Numerical experimentation has also shown that the residuals more closely approximate linear functions of $1/\gamma$ than γ. Therefore, the variable $\alpha = 1/\gamma$ is used as the sixth parameter.

The program must be supplied initial guesses for the parameters θ, a, and γ. The program will make its own guesses for the other parameters if none are supplied. The initial guess for X_0 is obtained by taking the average of the largest and the smallest X values found in the data. The initial guess for Z_0 is obtained by scanning the data for the point with the largest or smallest Z, depending upon the orientation of the drop. The initial guess for R_0 is taken to be half the drop width or the vertical distance between the apex and the widest place on the drop, whichever is larger.

Convergence is assumed when any of the following criteria are satisfied: (1) The largest element in $\mathbf{V}$ is smaller than ϵ_V (usually 10^{-7}). (2) The largest relative change in the physical parameters (θ, a, X_0, Z_0, R_0, γ) is smaller than ϵ_R (usually 10^{-7}). (3) The relative change in the objective function is smaller than ϵ_Q (usually 10^{-7}). (4) The directional derivative with respect to $\mathbf{V}$ of the objective function in the direction of steepest descent is smaller than ϵ_D (usually 10^{-7}). The ϵ values are read in with the input data. The program can be forced to accept convergence only on the basis of some subset of the above criteria by setting the other ϵ values to zero.

Computation of Confidence Limits

After the objective function has been minimized, confidence limits on the parameters are computed by using the formula for the approximate joint confidence region:[17]

$$(\mathbf{U}^c - \mathbf{U}^*)^T \boldsymbol{Q}''(\mathbf{U}^*) (\mathbf{U}^c - \mathbf{U}^*) = 2\sigma_r^2 n F_{1-\psi}(n,m-n)$$

or

$$\Delta\mathbf{U}^T \boldsymbol{Q}''(\mathbf{U}^*) \Delta\mathbf{U} = \Gamma \tag{27}$$

In eq 27 $\mathbf{U}^*$ is the solution to the minimization problem, $F_{1-\psi}(n,m-n)$ is the F test statistic for a confidence level of $1-\psi$ and $(n,m-n)$ degrees of freedom, and σ_r^2 is the sample variance of the residuals at the minimum:

$$\sigma_r^2 = Q(\mathbf{U}^*)/(m-n) \tag{28}$$

The elements of $\boldsymbol{Q}''$ are approximated by eq 18.

Equation 27 defines the approximate joint confidence region, $\mathbf{U}^c$. The approximate joint confidence region is an n-dimensional ellipsoid centered at the point $\mathbf{U}^*$ that has a probability of $1-\psi$ of containing the "true" parameter values (i.e., the values that would be obtained if there were no measurement error). The validity of the approximate joint confidence region is dependent upon the validity of the following assumptions: (1) The residuals are a random function of their position on the drop. (2) The residuals are normally distributed with a mean of zero. (3) $\mathbf{U}^*$ is a minimum of the objective function. (4) $\Delta\mathbf{U}$ is sufficiently small that the approximation of $\boldsymbol{Q}$ given by eq 18 is valid.

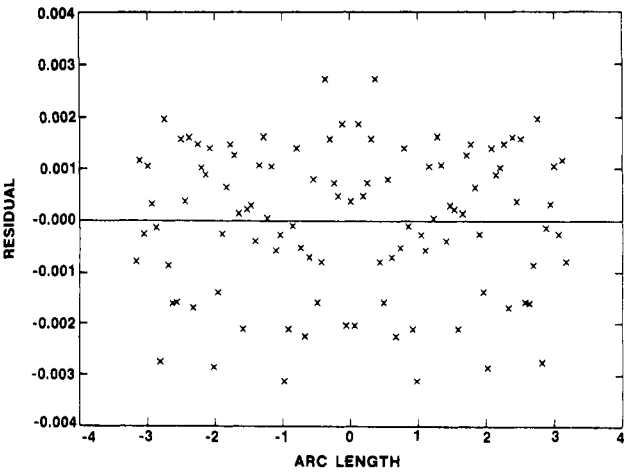

Figure 3. Plot of residuals from a fit of simulated experimental drop profile data as a function of position on the drop.

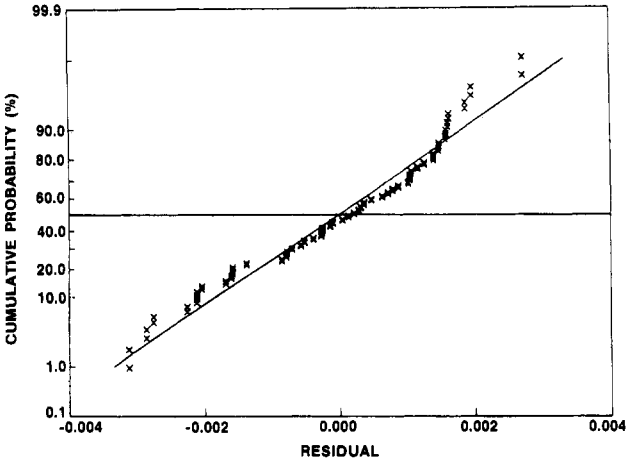

Figure 4. Plot of the cumulative probability of occurrence as a function of the residual from a fit of simulated experimental drop profile data.

Since the confidence region cannot be represented simply for a general n-dimensional problem, it will be helpful to compute the "outer" confidence limits. The outer confidence limit for the parameter k, ΔU_k^{out}, will be defined as the extrema of the ellipsoid with respect to the parameter U_k:

$$\Delta U_k^{out} = [\Gamma \sum_{i=1}^{n} (T_{ki}^2/E_{ii})]^{1/2} \tag{29}$$

A number of numerical experiments have been performed in order to verify the confidence limit calculations. In the first of these experiments a set of drop shape data, about 100 points equally spaced around the drop, was generated for a pendant drop. Measurement errors that may be encountered in the laboratory were simulated by overlaying the drop with a grid, representing a 500 × 500 pixel image system with an aspect ratio of 1, and rounding each data point to the nearest pixel. The confidence interval calculation involves the assumption that the residuals are random and normally distributed. This assumption has been tested by examining the residuals obtained by fitting the drop shape data described above. The residuals are plotted as a function of arc length from the apex in Figure 3. This figure is typical of similar figures that

(17) Himmelbau, D. M. *Process Analysis by Statistical Methods*; Sterling Swift: Austin, Texas, 1970.

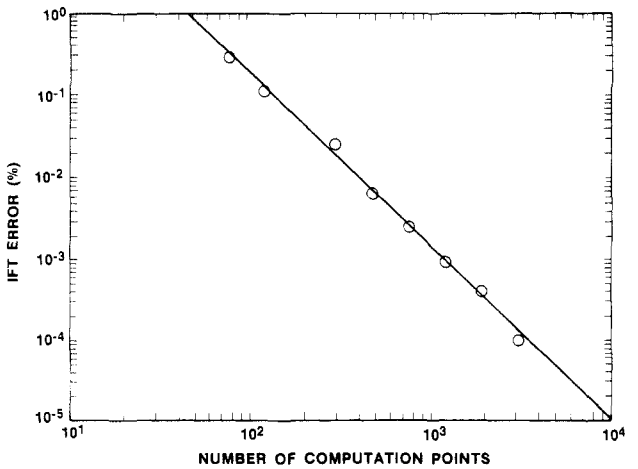

Figure 5. Plot of the error in IFT from a fit of an optimum pendant drop as a function of the number of computation points around the drop.

have been obtained for other drop shapes. It is considered adequate verification that the residuals are a random function of their position on the drop. The same residuals are plotted on probability coordinates in Figure 4, showing that they have an approximate Gaussian distribution.

The confidence limit calculation also involves the assumptions that the objective function can be approximated by an n-dimensional paraboloid and that the solution given by the minimization algorithm is indeed the minimum of the objective function. If these assumptions are accurate, the objective function will assume a constant value on the surface of the joint confidence region according to[16]

$$Q(\mathbf{U}^c) = Q(\mathbf{U}^*)[1 + (n/(m-n))F_{1-\psi}(n,m-n)] \quad (30)$$

When the objective function was evaluated at various points given by the confidence limit calculation it was found that eq 30 was satisfied to within 1%.

It should be pointed out that since the "outer" confidence intervals given by eq 29 are the extrema of the joint confidence region they define upper limits on the individual parameter confidence intervals. This implies that the computed confidence interval for interfacial tension gives a conservative estimate of the measurement accuracy. The actual accuracy is usually better than indicated by the error estimate.

Discussion of the Numerical Computation

The first test of the program was performed by using tabular drop shape data given by Padday[18] for both pendant and sessile drops as input data. Padday claims that his drop shape data, computed by a different numerical method than described in this paper, is accurate to four significant figures. The results for interfacial tension given by the program for a best fit of this data were also accurate to four significant figures. Thus, this first test also serves as a verification that the drop shape is being computed correctly.

In general, the accuracy of the drop shape computation and the residual computation increases as Δs is decreased. The computation time, however, also increases as Δs is decreased. The appropriate choice for Δs would be a value that was small enought to ensure the desired accuracy but not so small that excessive computer time is consumed. This choice has been determined through a simple numerical experiment. First a set of drop shape data was generated, about 100 points equally spaced around the drop, by using a very small Δs of about 0.0008 corresponding to about 10000 calculated points. This data set then was fit with the program by using a variety of values for Δs and recording the error in the determination of interfacial tension. The results are presented in Figure 5, which shows the percent error in γ as a function of the number of points used in the drop shape computation. The results shown in Figure 5 are for a pendant drop of optimum shape to be described later. However, very similar results are obtained for other drop shapes, including sessile drops.

The results show that the use of 1500 points will be more than adequate, giving an error in γ of about 0.001%.

(18) Padday, J. F. *Philos. Trans. R. Soc.* **1971**, *296*, 265.

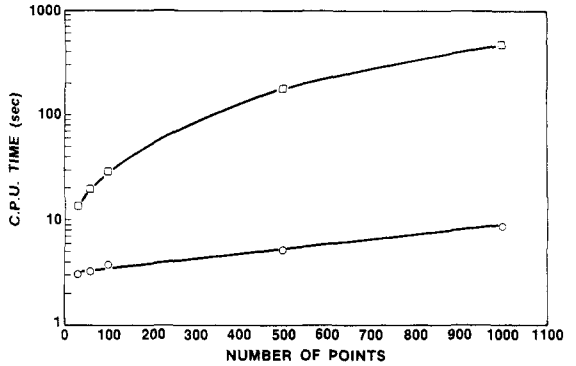

Figure 6. Plot of cpu time consumed to fit one sessile drop profile as a function of the number of coordinates by the method of ref 6, □, and the method of this work, ○, both with initial guesses and a VAX 8600 computer.

Time Study

In order to demonstrate the improved efficiency of the new program over that previously used,[6] sessile drop profile data sets of varying size were calculated. The data sets simulated data that have been obtained in this laboratory by using a computer-based image acquisition system to acquire and record the profiles. Typically, an error of ±0.0005 cm is found on each x,z coordinate. A typical data set may have several thousand coordinates with several hundred profiles recorded as a function of time.

The timing study was run with a calculated sessile drop profile with a contact angle of 110°, R_0 = 1.3634 cm, X_0 = Z_0 = 0.0000, γ = 72.79, $\Delta\rho$ = 0.99823, and g = 980.62. The amount of cpu time required to fit the data was recorded as a function of the number of coordinates in a single profile. The study was run on a VAX 8600 series computer. Figure 6 shows the results of this study. From these results we find that the previously reported routine requires approximately 54 times more cpu time for a 1000-coordinate profile than the routine reported here. For a data set consisting of 500 profiles each of 1000 coordinates, approximately 64 hours of cpu time would be required to complete the calculations with the program of Rotenberg et al.[6] as opposed to 70.25 min of cpu time with out routine. The savings in real time and expense to the experimentalist is obvious.

The Dependence of Error in the Interfacial Tension upon Drop Shape

All of the possible pendant (and emergent bubble) shapes can be uniquely specified by the dimensionless volume, V_d, the dimensionless radius at the syringe tip, R_d, and K, where

$$K = (\gamma/\Delta\rho g)^{1/2} \quad (31)$$

The parameter K has dimensions of length. The dimensionless tip radius is the tip radius divided by K, and the

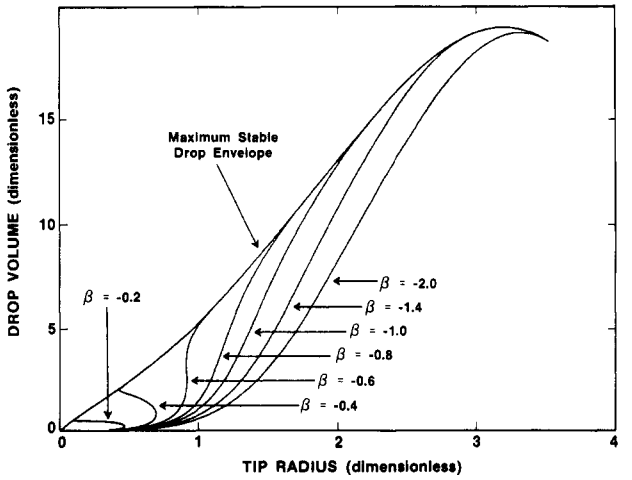

Figure 7. Stable pendant drops described by their dimensionless drop volume and dimensionless tip radii at several values of constant β.

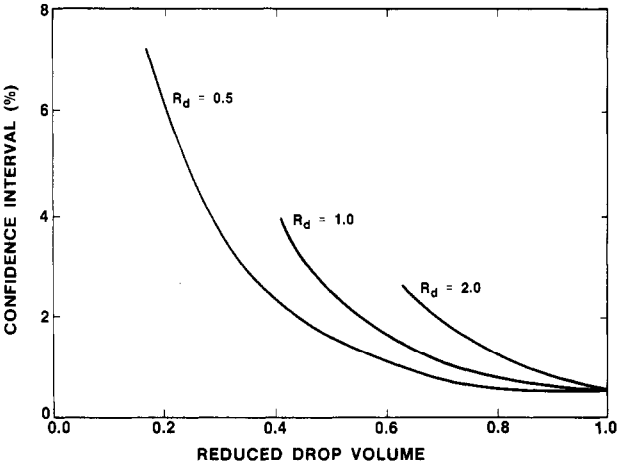

Figure 8. Effect of the reduced drop volume of pendant drops on the outer confidence interval for three dimensionless tip radii.

dimensionless drop volume is the drop volume divided by K^3. In Figure 7 V_d is plotted as a function of R_d for several values of constant β. These curves are bounded by an envelope that represents the maximum stable drop volume which can be obtained for any given tip radius under ideal conditions.[19]

A series of numerical experiments have been performed in order to determine which of the possible drop shapes lead to the most accurate determination of interfacial tension. This was accomplished by first generating a number of data sets for various drop shapes. Experimental measurement error was simulated, as described above, for a 500 × 500 pixel image system with an aspect ratio of 1. Before each data point was rounded to the nearest pixel a magnification factor was applied in order to exactly fill the image area, as would be done under ideal laboratory conditions. A best fit was then obtained for each data set, and the corresponding confidence intervals were recorded.

In Figure 8 the resulting confidence intervals, expressed as a percentage of the correct γ, are plotted as a function of reduced drop volume (the drop volume divided by the maximum stable drop volume at the same tip radius) for several values of constant R_d. This figure illustrates, as expected, that the largest possible stable drop for a given tip radius gives the most accurate determination of interfacial tension. In Figure 9 the confidence intervals are

(19) Padday, J. F. *Pure Appl. Chem.* **1976**, *48*, 485.

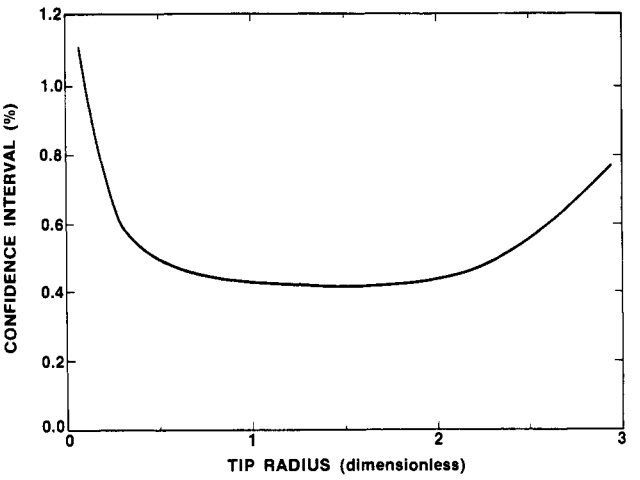

Figure 9. Effect of the dimensionless tip radius on the couter confidence interval for maximum stable pendant drops.

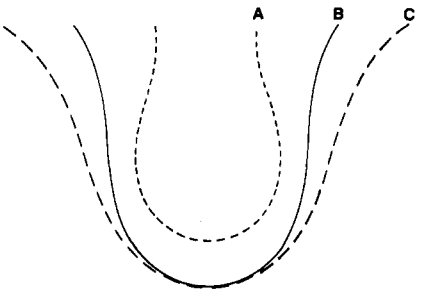

Figure 10. Shapes of three maximum stable pendant drops: (A) R_d = 0.5, (B) R_d = 1.3, (C) R_d = 2.0.

plotted as a function of R_d for a constant reduced drop volume of 1. From this figure it appears that the optimum range of pendant drop (or emergent bubble) shapes for the measurement of interfacial tension is the maximum stable drop for a dimensionless tip radius of about 0.8–2.0.

Interfacial tension measurements, using the shape-fitting method, can be made most accurately by using pendant drops in this range of shapes. It should be possible by using these drops to obtain 95% confidence intervals of about 0.4% for data sets of 100 points having an accuracy of 1 part in 500 (see Figure 9). Estimates of the uncertainty associated with data sets having a larger or smaller number of data points can be made by noting that the confidence intervals for a given drop shape are approximately inversely proportional to the square root of the number coordinates, as can be shown from eq 27. It can also be shown from eq 27 that for a given drop shape the uncertainty in interfacial tension measurement is proportional to the uncertainty in the coordinate point measurement.

It is also possible, of course, to make measurements by using drops outside of the optimum range. However, these measurements will be subject to additional uncertainty, which can be estimated from Figures 8 and 9.

The shapes of three maximum stable drops are illustrated in Figure 10, two inside the optimum range (R_d = 1.3, 2.0) and one outside (R_d = 0.5). This figure clearly demonstrates that a maximum volume stable pendant drop need not have an equatorial diameter. Such a pendant drop would of course be entirely unsuitable for analysis by the method of selected plane. Since an equatorial diameter is not necessary for the shape-fitting method, an optimum drop shape may be obtained with a tip radius significantly larger than is usually required in pendant drop interfacial tension measurement. This fact is important since it reduces the range of syringe tip sizes re-

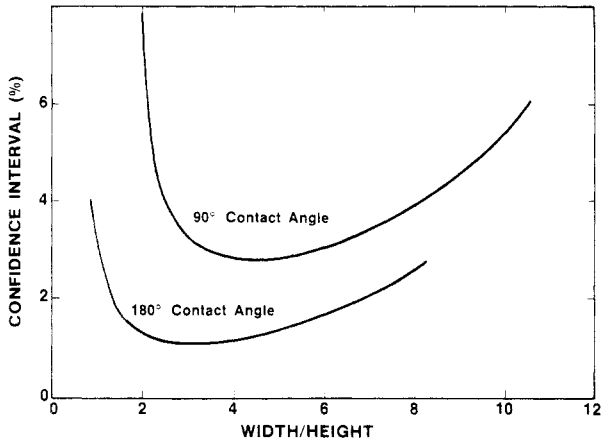

Figure 11. Effect of the drop width to height ratio on the outer confidence interval for sessile drops with two different contact angles.

Table I. (X,Z) Coordinate Data for Water at 25 °C[a]

X	Z	X	Z	X	Z
2.6559	7.7718	2.8121	6.2628	4.1982	6.9404
2.5709	7.5786	2.9157	6.1912	4.2017	6.9984
2.4905	7.3004	3.0595	6.1238	4.2009	7.1084
2.4735	7.1977	3.3403	6.0773	4.1923	7.1977
2.4661	7.1084	3.6060	6.1238	4.1760	7.3004
2.4646	6.9984	3.7504	6.1912	4.0933	7.5786
2.4683	6.9404	3.8551	6.2628	4.0095	7.7718
2.4840	6.8255	4.1418	6.6758	3.9471	7.8973
2.5237	6.6758	4.1820	6.8255	3.8697	8.0481
2.5897	6.5307				

[a] Magnification = 5.2038; coordinates are $\pm 2 \times 10^{-4}$ cm.

quired for measurement of large interfacial tension ranges.

It must be noted that this analysis has been performed with the assumption of ideal conditions. In practice, it may be more difficult to approach the maximum drop volume for larger tips. It should also be noted that the analysis has been conducted with the assumption that the aspect ratio of the image system is equal to 1. For an image system with an aspect ratio not equal to 1 there will probably be a broader range of optimum drop shapes. This is due to the fact that maximum use of the image area can be obtained by turning the camera 90°, if necessary, in order to align the largest dimension of the image area with the largest dimension of the drop.

A similar analysis has been performed for sessile drops and captive bubbles. Under the same ideal conditions the optimum sessile drop appears to be a drop with a contact angle of 180° and a width about 3 times its height (see Figure 11). However, this optimum sessile drop does not lead to as accurate a measurement of interfacial tension as the optimum pendant drop, giving confidence limits between 2 and 3 times larger.

Comparison of Techniques

As an example of the use of the program we have developed, we present data and the analyses for a drop of water against water vapor saturated nitrogen at 25 °C. The water was prepared as previously reported.[20] The drop profile coordinates were recorded from a photographic negative, Kodak Technical pan film developed with a high contrast D19 developer, by using a Gaetner coordinate cathetometer. The apparatus and experimental detals will be reported elsewhere. The raw data are presented in Table I. In order to facilitate comparison with other

(20) Pallas, N. R.; Pethica, B. A. *Colloids Surf.* **1983**, *6*, 221.

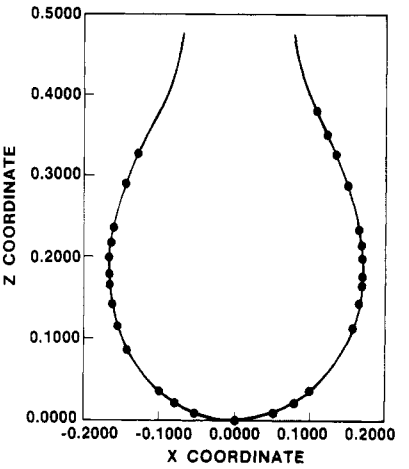

Figure 12. Computed drop shape, solid line, compared to the input data, ●, for a drop of water at 25 °C as analyzed by the technique presented in this work.

Table II. Analyses of Data Shown in Table I

method	interfacial tension, dyn/cm	error estimate, dyn/cm
this work	72.10	$71.79 \leq \gamma \leq 72.42$
ref 6	72.10	$71.94 \leq \gamma \leq 72.08$
ref 4	72.16	$71.46 \leq \gamma \leq 72.86$

published results this example data set is composed of a relatively small number of coordinates collected manually. However, the analysis method is usually used with much larger data sets collected by using a digital image analysis system.

The data were analyzed by three techniques: that presented here, the technique of Rottenberg, Boruvka, and Neumann,[6] and the selected plane method of Roe, Bachetta, and Wong.[4] The results of the analysis are presented in Table II. Figure 12 shows a plot of the calculated and observed data as analyzed by the technique herein presented. Generally, the results of the three analyses agree well with each other and with the literature value of 72.0 ± 0.1 dyn cm^{-1}.[20] It should be noted that the confidence limit range given by the method of Rottenberg et al.[6] does not bracket the mean. The error estimate on the method of ref 4 is simply the range of values about the average.

Acknowledgment. We thank The Standard Oil Production Co. and the Standard Alaska Production Co. for permission to publish this work, Y. Gibson-Robinson for work on part of this project, Dr. M. J. King for his assistance in the preparation of the manuscript, Dr. J. S. Nolen for use of his notes on the method of rotational discrimination, and G. Taylor for the typing of the manuscript.

Appendix

The partial derivatives of the residuals with respect to the elements of **U** are derived as follows. From eq 12 we have

$$\partial r_i/\partial U_1 = (\partial r_i/\partial \theta)w_\theta; \qquad \partial r_i/\partial U_2 = (\partial r_i/\partial a)w_a;$$
$$\partial r_i/\partial U_3 = (\partial r_i/\partial X_0)w_X;$$
$$\partial r_i/\partial U_4 = (\partial r_i/\partial Z_0)w_Z; \qquad \text{(A1)}$$
$$\partial r_i/\partial U_5 = (\partial r_i/\partial R_0)w_R; \qquad \partial r_i/\partial U_6 = (\partial r_i/\partial \alpha)w_\alpha$$

Differentiating eq 10 with respect to θ yields

$$\frac{\partial r_i}{\partial \theta} = -\frac{1}{r_i}\left[(X(s_i) - X_i)\frac{\partial X_i}{\partial \theta} + (Z(s_i) - Z_i)\frac{\partial Z_i}{\partial \theta}\right] \qquad \text{(A2)}$$

From eq 8 we have

$$\partial X_i/\partial\theta = -(X_i^{obsd}/M_x - X_0)\sin\theta + (aZ_i^{obsd}/M_z - Z_0)\cos\theta = Z_i$$

$$\partial Z_i/\partial\theta = -(aZ_i^{obsd}/M_z - Z_0)\sin\theta - (X_i^{obsd}/M_x - X_0)\cos\theta = -X_i \quad (A3)$$

Hence

$$\partial r_i/\partial\theta = (1/r_i)[(Z(s_i) - Z_i)X_i - (X(s_i) - X_i)Z_i] \quad (A4)$$

Similarly, it can be shown that

$$\frac{\partial r_i}{\partial a} = -\frac{1}{r_i}\frac{Z_i^{obsd}}{M_x}[(X(s_i) - X_i)\sin\theta + (Z(s_i) - Z_i)\cos\theta]$$

$$\frac{\partial r_i}{\partial X_0} = \frac{1}{r_i}[(X(s_i) - X_i)\cos\theta - (Z(s_i) - Z_i)\sin\theta]$$

$$\frac{\partial r_i}{\partial Z_0} = \frac{1}{r_i}[(X(s_i) - X_i)\sin\theta + (Z(s_i) - Z_i)\cos\theta] \quad (A5)$$

Differentiating eq 10 with respect to R_0 yields the following equation:

$$\frac{\partial r_i}{\partial R_0} = \frac{1}{r_i}\left[(X(S_i) - X_i)\times\left(x(s_i) + R_0\frac{\partial x(s_i)}{\partial R_0}\right) + (Z(s_i) - Z_i)\left(z(s_i) + R_0\frac{\partial z(s_i)}{\partial R_0}\right)\right] \quad (A6)$$

Using the definitions of x', z', and β one obtains

$$\frac{\partial x(s_i)}{\partial R_0} = \frac{\partial x(s_i)}{\partial\beta}\frac{\partial\beta}{\partial R_0} = \frac{2\beta}{R_0}x'(s_i)$$

$$\frac{\partial z(s_i)}{\partial R_0} = \frac{\partial z(s_i)}{\partial\beta}\frac{\partial\beta}{\partial R_0} = \frac{2\beta}{R_0}z'(s_i) \quad (A7)$$

Hence

$$\frac{\partial r_i}{\partial R_0} = \frac{1}{r_i}[(X(s_i) - X_i)(x(s_i) + 2\beta x'(s_i)) + (Z(s_i) - Z_i)\times(z(s_i) + 2\beta z'(s_i))] \quad (A8)$$

Similarly, it can be shown that

$$\frac{\partial r_i}{\partial\alpha} = \frac{\beta R_0}{r_i\alpha}[(X(s_i) - X_i)x'(s_i) + (Z(s_i) - Z_i)z'(s_i)] \quad (A9)$$

The values for $x(s_i)$, $x'(s_i)$, $z(s_i)$, and $z'(s_i)$ may be easily approximated by an appropriate linear interpolation between their values at the points (X_j,Z_j) and (X_{j+1},Z_{j+1}).

Dye Sensitization of van der Waals Surfaces of SnS_2 Photoanodes†

B. A. Parkinson

E.I. du Pont de Nemours & Co., Central Research and Development Department, Experimental Station E328/216B, Wilmington, Delaware 19898

Received February 15, 1988. In Final Form: April 5, 1988

The sensitization of the van der Waals surface of SnS_2 (E_g = 2.22 eV) with over 30 different dyes (λ_{max} < 2.2 eV) is studied. The van der Waals surface of this material has several advantages for studying sensitization. It is renewable via cleavage and lacks an oxide layer under ambient conditions. The relevance of the electrochemical properties of the dyes to their sensitization behavior is discussed. Adsorption isotherms for many of the dyes were measured by relating quantum yield for electron injection to surface coverage. Both J and H aggregates and monomeric dye species sensitize n-SnS_2. The photocurrent–voltage behavior of the dye is interpreted by using Spitler's theory of electron injection into semiconductors. Sensitized photocurrents are also studied as a function of light intensity and supersensitizer concentration to aid the qualitative theoretical analysis. Several unusual effects associated with the layered structure of the semiconductor are observed including dye intercalation, total internal reflection of the incident light, and surface phase changes.

Introduction

The sensitization of a silver halide grain via electron injection from a highly absorbing organic dye molecule is the process underlying photography.[1,2] Adsorption of dye molecules onto the surface of semiconductor electrodes has for many years been used to model sensitization of silver halides and as a potential method of energy conversion.[3-13] The semiconductor is sensitized to sub-band-gap light via electron injection into the conduction band of the semiconductor from the excited state of the dye molecule with the overall efficiency of the process directly measurable via the photocurrent. Understanding of dye and dye aggregate sensitization efficiency, of the excited states involved in injection, and of the energetic thresholds for electron injection has mostly resulted from photoelectrochemical and spectroscopic studies of oxide semiconductors

†Contribution No. 4685 from E. I. du Pont de Nemours & Co.

(1) *The Theory of the Photographic Process, 4th ed.*; James, T. H., Ed.; MacMillan: New York, 1977.
(2) Berriman, R. W.; Gilman, P. B., Jr. *Photogr. Sci. Eng.* **1973**, *17*, 235.
(3) Gerischer, H.; Tributsch, H. *Ber. Bunsen-Ges. Phys. Chem.* **1968**, *72*, 437.
(4) Memming, R.; Tributsch, H. *J. Phys. Chem.* **1971**, *75*, 562.
(5) Memming, R. *Photochem. Photobiol.* **1972**, *16*, 325.
(6) (a) Gerischer, H.; Willig, F. In *Topics in Current Chemistry*; Davison, A., Ed.; Springer: New York, 1976; pp 61, 31. (b) Gerischer, H.; Spitler, M. T.; Willig, F. In *Electrode Processes 1979*; Bruckenstein, S., Ed.; Electrochemical Society: Princeton, NJ, 1980, p 115.
(7) Sonntag, L. P.; Spitler, M. T. *J. Phys. Chem.* **1985**, *89*, 1453.
(8) Natoli, L. M.; Ryan, M. A.; Spitler, M. T. *J. Phys. Chem.* **1985**, *89*, 1448.
(9) Spitler, M. T.; Calvin, M. *J. Chem. Phys.* **1977**, *66*, 4294.
(10) Spitler, M. T.; Calvin, M. *J. Chem. Phys.* **1977**, *67*, 5193.

0743-7463/88/2404-0967$01.50/0